Bound-state soliton gas as a limit of adiabatically growing integrable turbulence

Dmitry Agafontsev[1,2], Andrey Gelash[2,3], Rustam Mullyadzhanov[4,5], Vladimir Zakharov[6]

[1] Shirshov Institute of Oceanology of RAS, Moscow, Russia

[2] Skolkovo Institute of Science and Technology, Moscow, Russia

[3] Institute of Automation and Electrometry SB RAS, Novosibirsk, Russia.

[4] Institute of Thermophysics SB RAS, Novosibirsk, Russia.

[5] Novosibirsk State University, Novosibirsk, Russia.

[6] Department of Mathematics, University of Arizona, Tucson, USA.

XXXI Scientific Session of the RAS Council on Nonlinear Dynamics

Shirshov Institute of Oceanology of RAS
19-20 December 2022.

1. Formulation of the problem (1).

We study the long-time statistics of solutions to the following dimensionless problem,

$$\psi_{t=0} = A_0 f(x), \quad \overline{|f|^2} = 1, \tag{1}$$

$$\begin{cases} i\psi_t + \psi_{xx} + |\psi|^2\psi = ip_0\psi, & \text{while} \quad \overline{|\psi|^2} < A_f^2, \\ i\psi_t + \psi_{xx} + |\psi|^2\psi = 0, & \text{for} \quad \overline{|\psi|^2} = A_f^2, \end{cases} \tag{2}$$

where the function $f(x)$ has unit average intensity and unit characteristic spatial scale $\delta x = 1$, the coefficients A_0 and A_f are the initial and final mean amplitudes, and p_0 is the renormalized pumping coefficient. The overline denotes spatial averaging,

$$\overline{|f|^2} = \frac{1}{L}\int_{-L/2}^{L/2} |f|^2\, dx,$$

over the simulation box $x \in [-L/2, L/2]$ with periodic boundary; the period (basin length) is considered to be large, $L \gg \delta x = 1$.

Hence, our results may depend on (i) initial and final mean amplitudes A_0 and A_f, (ii) noise statistics given by the function $f(x)$, (iii) pumping coefficient p_0 and (iv) box size L.

Our work contains two major parts. In the first part, we study statistical characteristics of wavefield examining the basic statistical function such as Fourier spectrum, probability density function of intensity and autocorrelation of intensity. In the second part, we solve the direct Zakharov-Shabat scattering problem for the grown-up wavefields and examine their inverse scattering (IST) spectra.

1. Formulation of the problem (2).

For adiabatic growth of turbulence, which goes sequentially through the statistically stationary states of the integrable turbulence, we need to ensure that (i) the pumping is small, so that the motion is governed primarily by the terms of the 1D-NLSE, and (ii) the initial state is already close to stationary. The latter is possible if the initial wavefield is almost linear (e.g. small noise), because the linear turbulence is stationary.

It is also instructive to consider the equation of motion (2) in the Fourier space,

$$i\frac{\partial \psi_k}{\partial t} - k^2\psi_k + (|\psi|^2\psi)_k = ip_0\psi_k, \tag{3}$$

where $(|\psi|^2\psi)_k$ is the Fourier-transformed nonlinear term of the 1D-NLSE. For adiabatic growth of turbulence, we need to ensure that the pumping term is much smaller than all the other terms present in the equation, including the dispersion term where there is an explicit dependency on the wavenumber k. This must be satisfied for all wavenumbers, including the smallest nonzero ones $k = \pm\Delta k = \pm 2\pi/L$, i.e.,

$$p_0 \ll \left(\frac{2\pi}{L}\right)^2 \quad \leftrightarrow \quad L \ll \frac{2\pi}{\sqrt{p_0}}. \tag{4}$$

In total, the conditions for adiabatic growth can be summarized as

$$p_0 \ll \left(\frac{2\pi}{L}\right)^2, \quad A_0^2 \ll 1. \tag{5}$$

Our experiments indicate that when these conditions are met, the turbulence indeed grows adiabatically.

2. Numerical methods.

We use Runge-Kutta 4th order method on adaptive grid combined with Fourier interpolation between the grids. For more accurate simulation of the growth stage, we rewrite the 1D-NLSE for the function $v = e^{-p_0 t} \cdot \psi$, eliminating the right-hand side of the equation. After turning off the pumping, we have checked that the first ten integrals of motion are conserved by our numerical scheme up to the relative errors from 10^{-10} (the first three invariants) to 10^{-6} (the tenth invariant) orders.

The function $f(x)$, that defines statistics of the initial noise in Eq. (1) and has unit average intensity and unit characteristic spatial scale, is constructed as superposition of linear waves,

$$f(x) = \sum_k F_k \, e^{ikx + i\phi_k}, \quad F_k = G_s \, e^{-|k|^s}. \tag{6}$$

Here $s \in \mathbb{N}$ is the exponent defining shape of the Fourier spectrum F_k, ϕ_k are random phases for each k and each realization of the initial noise, $G_s = [\pi \, 2^{1/s} / L \, \Gamma_{1+1/s}]^{1/2}$ is the normalization constant such that the average intensity is unity, $\overline{|f|^2} = 1$, L is the basin length, and Γ is the Euler Gamma-function.

Base experiment (adiabatic regime): $L = 128\pi$, $s = 2$, $A_0 = 10^{-2}$, $A_f = 1$ and $p_0 = 10^{-5}$.

For each of the several numerical experiments presented in this paper, we perform simulations of time evolution in the formulation of Eqs. (1)-(2) for an ensemble of several hundred realizations of the initial noise, which differ only in the set of random Fourier phases ϕ_k in Eq. (6), and then average the statistical results over these realizations. We have checked that larger ensemble sizes lead to the same statistical results.

3. Results (wave statistics): stationary state (1).

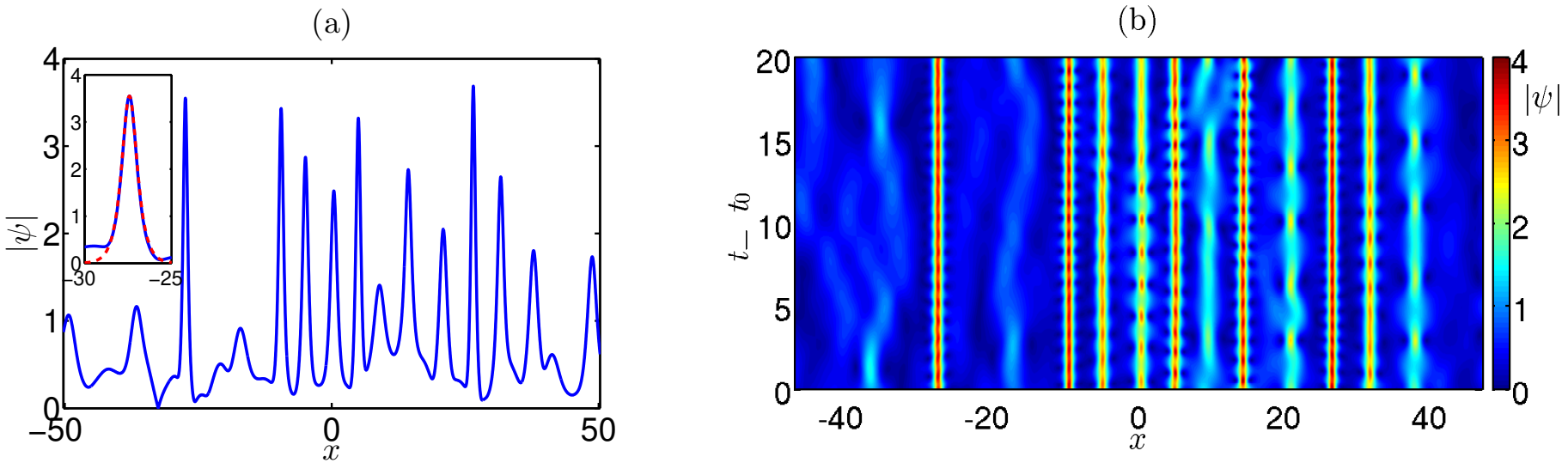

Figure 1: (a) Amplitude $|\psi|$ for a single realization of wavefield at the end of the growth stage $t = t_0$ and (b) its subsequent space-time evolution after turning off the pumping, $t \geq t_0$. The parameters correspond to the base numerical experiment: $L = 128\pi$, $s = 2$, $A_0 = 10^{-2}$, $A_f = 1$ and $p_0 = 10^{-5}$. The inset in panel (a) shows fit for one of the pulses with the one-soliton solution. Note that both panels demonstrate only the central quarter of the basin length.

The one-soliton solution of the 1D-NLSE can be written as,

$$\psi_s(x,t) = \chi \frac{\exp\left[iV(x-x') + i\theta'\right]}{\cosh \chi\,(x-x')}, \quad x' = x_0' + Vt, \quad \theta' = \theta_0' + \frac{1}{2}(\chi^2 + V^2)t,$$

where $\chi > 0$, V, x' and θ' are real-valued soliton amplitude, velocity and current position and phase, while the constants x_0' and θ_0' stand for the position and phase at $t = 0$.

3. Results (wave statistics): stationary state (2).

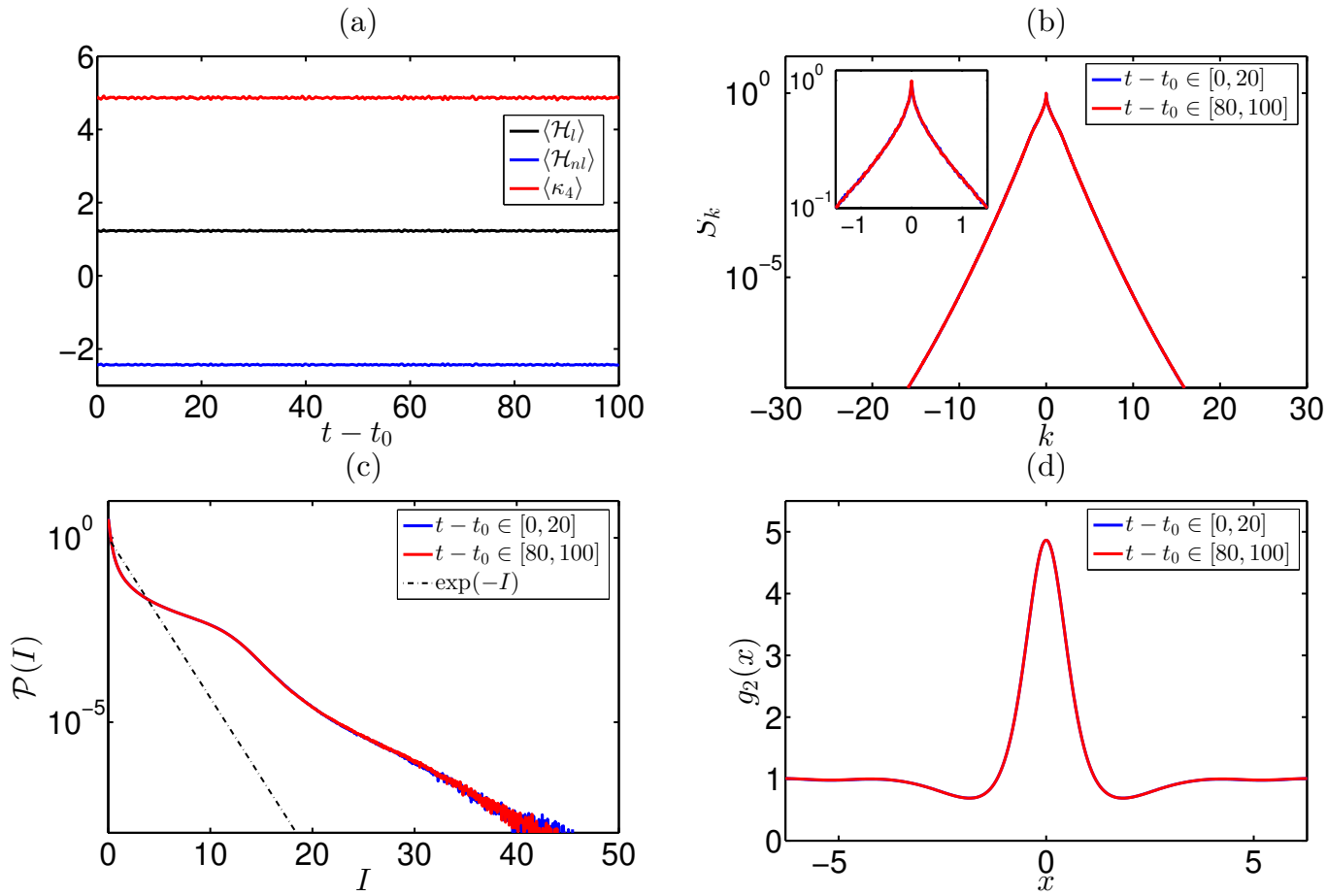

Figure 2: (a) Evolution of the ensemble-averaged kinetic energy $\langle \mathcal{H}_l \rangle$, potential energy $\langle \mathcal{H}_{nl} \rangle$ and fourth-order moment of amplitude κ_4 after turning off the pumping, $t \geq t_0$. (b-d) Statistical functions averaged over the ensemble and different time intervals $t - t_0 \in [0, 20]$ and $t - t_0 \in [80, 100]$: (b) the wave-action spectrum S_k, (c) the PDF $\mathcal{P}(I)$ of relative wave intensity $I = |\psi|^2 / \langle |\psi|^2 \rangle$ and (d) the autocorrelation of intensity $g_2(x)$. The base numerical experiment: $L = 128\pi$, $s = 2$, $A_0 = 10^{-2}$, $A_f = 1$ and $p_0 = 10^{-5}$.

3. Results (wave statistics): adiabatic regime.

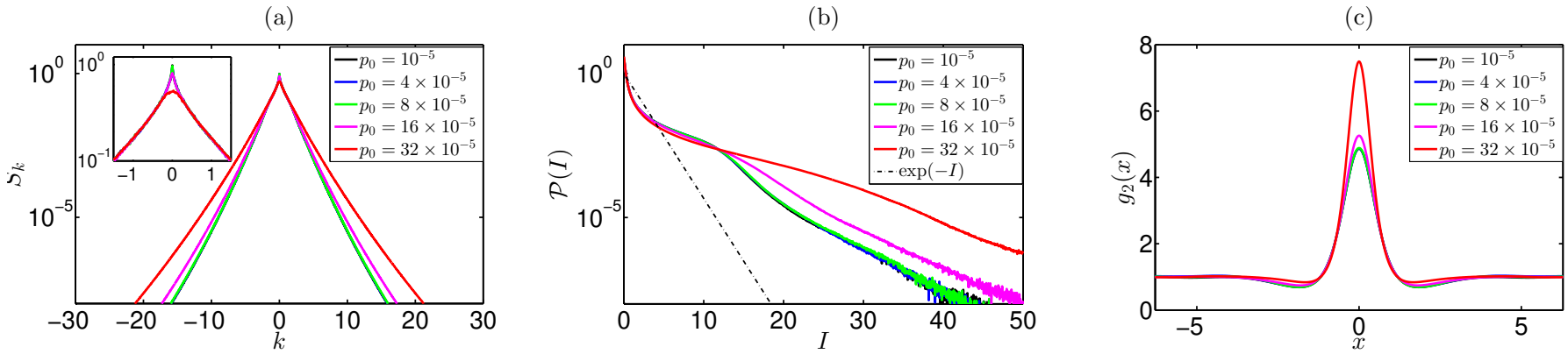

Figure 3: Statistical functions averaged over the ensemble and time interval $t - t_0 \in [0, 20]$ for the experiments with different pumping coefficients p_0 and fixed $A_0 = 10^{-2}$ and $L = 128\pi$: (a) the wave-action spectrum S_k, (b) the PDF $\mathcal{P}(I)$ of relative wave intensity $I = |\psi|^2/\langle|\psi|^2\rangle$ and (c) the autocorrelation of intensity $g_2(x)$. The initial spectrum is Gaussian, $s = 2$, and the final average amplitude equals unity, $A_f = 1$.

The conditions of adiabaticity:

$$p_0 \ll \left(\frac{2\pi}{L}\right)^2 \leftrightarrow L \ll \frac{2\pi}{\sqrt{p_0}}, \qquad A_0^2 \ll 1.$$

Experiments with $p_0 \leq 8 \times 10^{-5}$ demonstrate adiabatic regime of the turbulence growth.

3. Results (wave statistics): universal adiabatic regime.

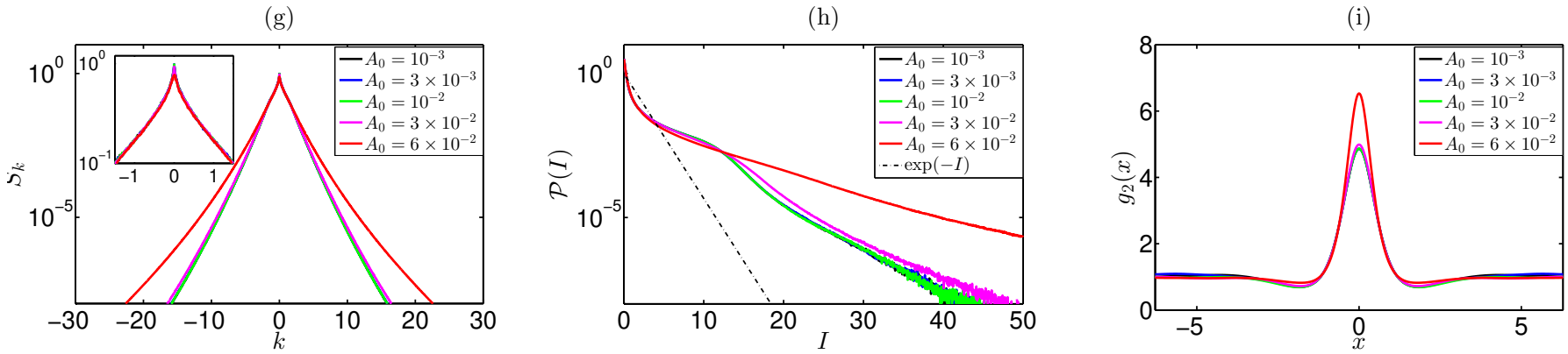

Figure 4: Statistical functions averaged over the ensemble and time interval $t - t_0 \in [0, 20]$ for the experiments with different initial amplitudes A_0 and fixed $p_0 = 10^{-5}$ and $L = 128\pi$: (g) the wave-action spectrum S_k, (h) the PDF $\mathcal{P}(I)$ of relative wave intensity $I = |\psi|^2 / \langle |\psi|^2 \rangle$ and (i) the autocorrelation of intensity $g_2(x)$. The initial spectrum is Gaussian, $s = 2$, and the final average amplitude equals unity, $A_f = 1$.

From here we can introduce the notions of universal and non-universal adiabatic regimes: the universal regime is the regime when decreasing the initial noise amplitude A_0 doesn't lead to changes in statistics, and the non-universal one is the regime when it does.

The study of IST spectra shows that starting from $A_0 \geq 3 \times 10^{-2}$ solitons start to appear in the initial noise (1-2 for some noise realizations), while for $A_0 \leq 10^{-2}$ they are absent.

3. Results (wave statistics): dependency on initial spectrum.

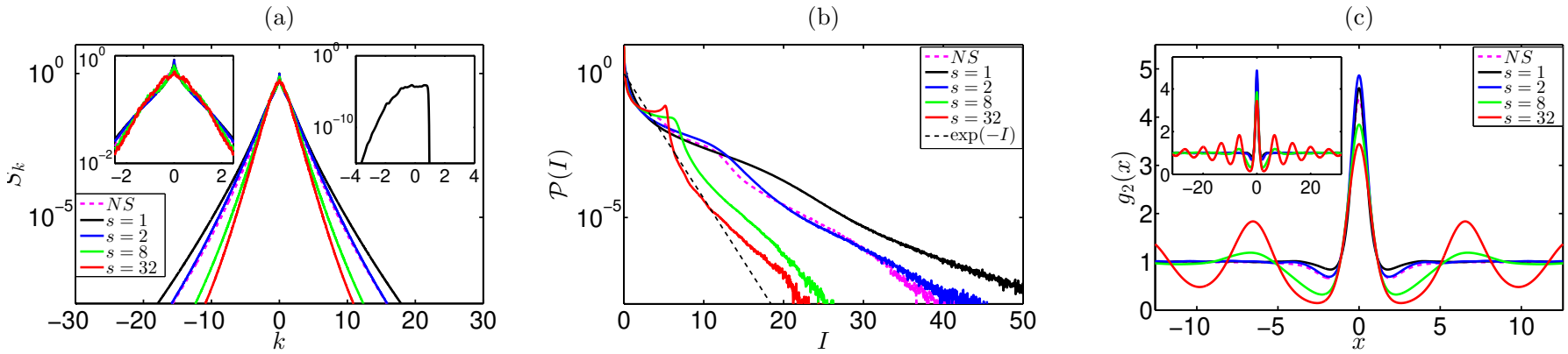

Figure 5: Statistical functions averaged over the ensemble and time interval $t - t_0 \in [0, 20]$ for four super-Gaussian initial spectra with the exponents $s = 1$, 2, 8 and 32, and one non-symmetric initial spectrum *NS*: (a) the wave-action spectrum S_k, (b) the PDF $\mathcal{P}(I)$ of relative wave intensity $I = |\psi|^2/\langle|\psi|^2\rangle$ and (c) the autocorrelation of intensity $g_2(x)$. The other parameters are the same as for the base experiment: $L = 128\pi$, $A_0 = 10^{-2}$, $A_f = 1$ and $p_0 = 10^{-5}$.

The function $f(x)$, that defines statistics of the initial noise in Eq. (1) and has unit average intensity and unit characteristic spatial scale, is constructed as superposition of linear waves,

$$f(x) = \sum_k F_k \, e^{ikx + i\phi_k}, \quad F_k = G_s \, e^{-|k|^s}.$$

Here $s \in \mathbb{N}$ is the exponent defining shape of the Fourier spectrum F_k, ϕ_k are random phases for each k and each realization of the initial noise, $G_s = [\pi \, 2^{1/s}/L\,\Gamma_{1+1/s}]^{1/2}$ is the normalization constant such that the average intensity is unity, $\overline{|f|^2} = 1$, L is the basin length, and Γ is the Euler Gamma-function.

3. Results (wave statistics): dependency on final amplitude A_f.

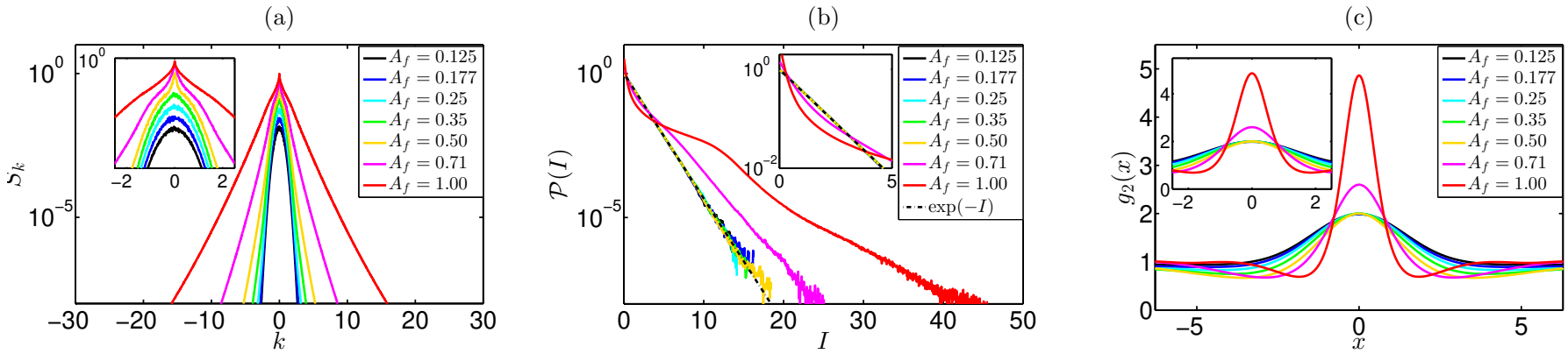

Figure 6: Statistical functions averaged over the ensemble and time interval $t - t_0 \in [0, 20]$ at different average amplitudes $A_f = 0.125$, 0.177, 0.25, 0.35, 0.5, 0.71 and 1: (a) the wave-action spectrum S_k, (b) the PDF $\mathcal{P}(I)$ of relative wave intensity $I = |\psi|^2/\langle\overline{|\psi|^2}\rangle$ and (c) the autocorrelation of intensity $g_2(x)$. All the other parameters correspond to the base experiment: $L = 128\pi$, $s = 2$, $A_0 = 10^{-2}$ and $p_0 = 10^{-5}$.

Potential-to-kinetic energy ratio $\alpha = \langle|\mathcal{H}_{nl}|\rangle/\langle\mathcal{H}_l\rangle$ vs. mean amplitude A_f:

$A_f = 0.125$ $\alpha = 0.0625$,
$A_f = 0.177$ $\alpha = 0.125$,
$A_f = 0.250$ $\alpha = 0.25$,
$A_f = 0.354$ $\alpha = 0.5$,
$A_f = 0.500$ $\alpha = 1$,
$A_f = 0.707$ $\alpha = 1.74$,
$A_f = 1.000$ $\alpha = 1.98$.

4. Results – IST spectra, adiabatic regime (1).

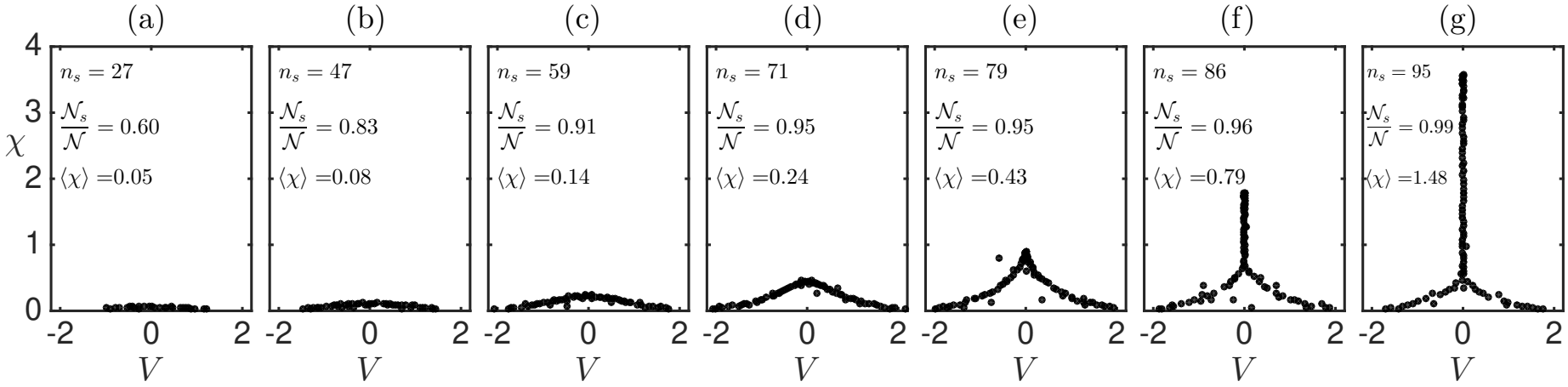

Figure 7: Amplitude-velocity diagrams of solitons for simulation from a single realization of initial conditions at different stages of the pumping: (a) $A_f = 0.125$, (b) $A_f = 0.177$, (c) $A_f = 0.25$, (d) $A_f = 0.35$, (e) $A_f = 0.5$, (f) $A_f = 0.71$ and (g) $A_f = 1$. The parameters correspond to the base experiment: $L = 128\pi$, $s = 2$, $A_0 = 10^{-2}$ and $p_0 = 10^{-5}$; panel (g) refers to the wavefield from Fig. 1(a). Each dot represents a soliton within the studied wavefield, n_s shows total number of solitons detected, $\mathcal{N}_s/\mathcal{N}$ demonstrates ratio between the wave action of the solitonic part $\mathcal{N}_s$ and the total wave action $\mathcal{N}$, and $\langle\chi\rangle$ indicates the mean soliton amplitude.

4. Results – IST spectra, adiabatic regime (2).

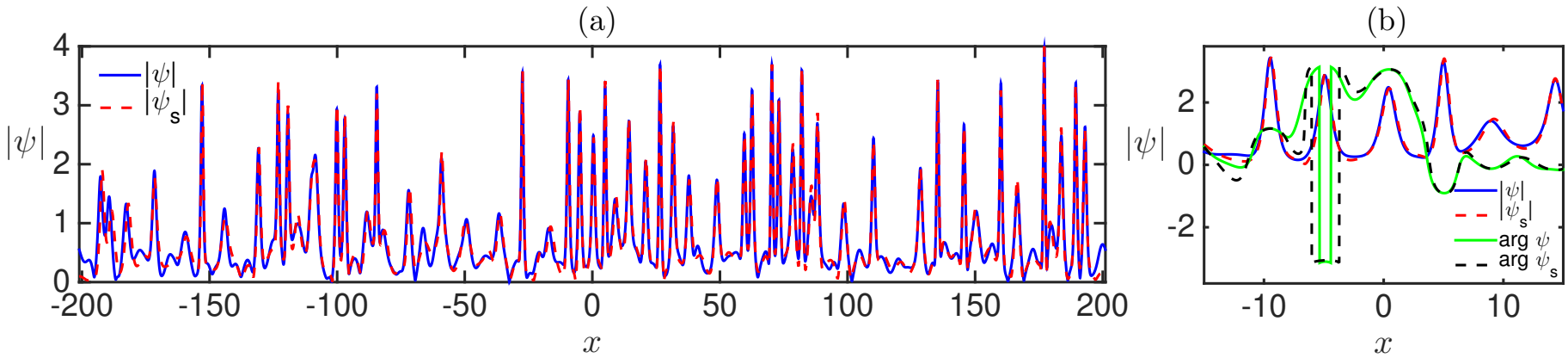

Figure 8: Typical grown-up wavefield and its approximation with the multi-soliton solution ψ_s generated from the discrete part of the scattering data, for the base numerical experiment with parameters $L = 128\pi$, $s = 2$, $A_0 = 10^{-2}$, $A_f = 1$ and $p_0 = 10^{-5}$. Panel (a) shows absolute value $|\psi|$ of the grown-up wavefield (solid blue) and multi-soliton solution (dashed red), while panel (b) represents zoom of panel (a) at the central region. Also, panel (b) illustrates complex phase $\arg\psi$ of the grown-up wavefield (solid green) and multi-soliton solution (dashed black). Note that panel (a) shows the same grown-up wavefield as in Fig. 1(a), but over the entire basin length.

4. Results – IST spectra, adiabatic regime (3).

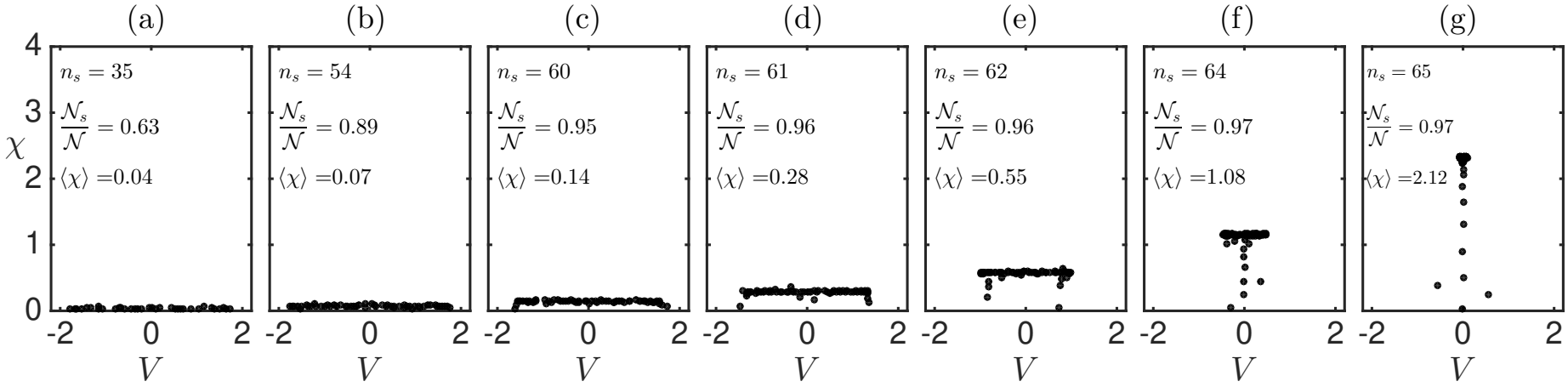

Figure 9: Amplitude-velocity diagrams of solitons for simulation from a single realization of initial conditions at different stages of the pumping. The parameters are: $L = 128\pi$, $s = 32$, $A_0 = 10^{-2}$ and $p_0 = 10^{-5}$.

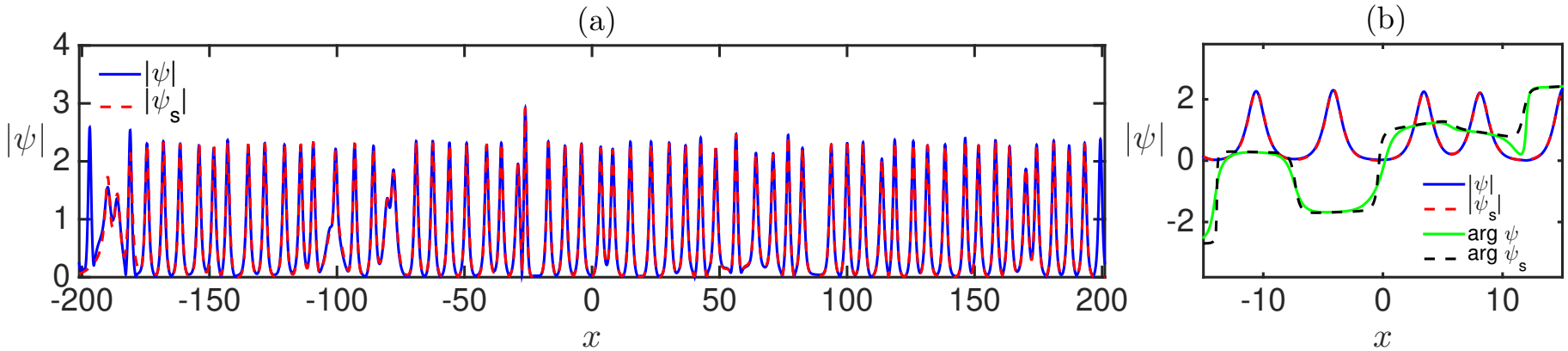

Figure 10: Typical grown-up wavefield and its approximation with the multi-soliton solution ψ_s; the parameters are $L = 128\pi$, $s = 32$, $A_0 = 10^{-2}$, $A_f = 1$ and $p_0 = 10^{-5}$.

4. Results – IST spectra, adiabatic regime (4).

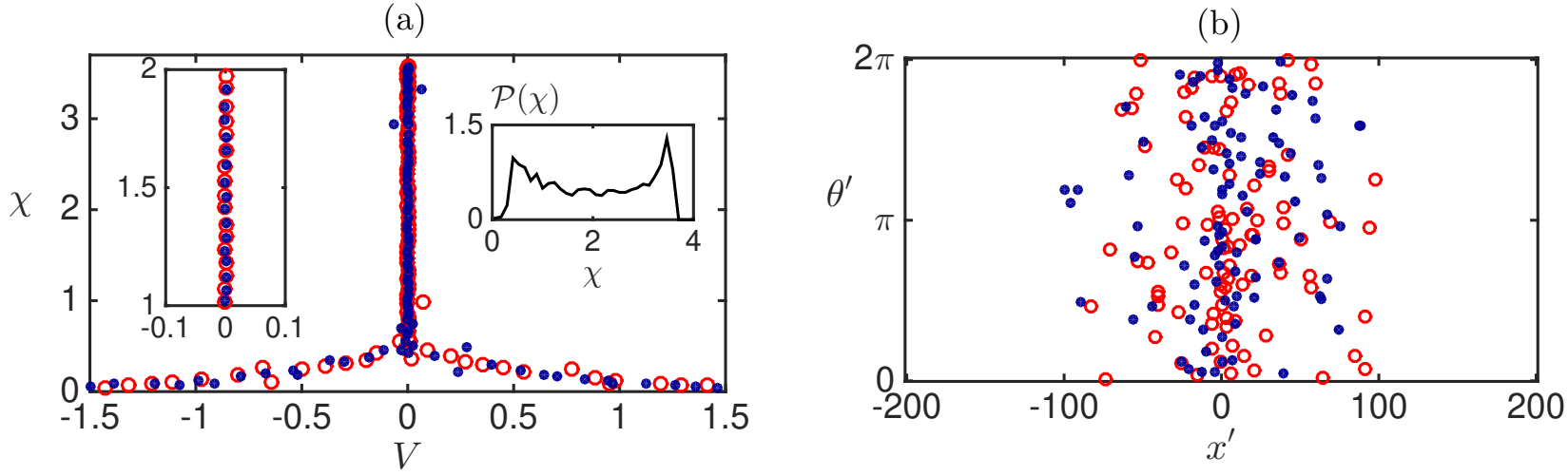

Figure 11: Soliton diagrams for the base numerical experiment with parameters $L = 128\pi$, $s = 2$, $A_0 = 10^{-2}$, $A_f = 1$ and $p_0 = 10^{-5}$: (a) for amplitudes χ and velocities V, and (b) for positions x' and phases θ'. Blue dots and red circles represent solitons for two different realizations of the grown-up wavefield. The left inset in panel (a) shows zoom of the main figure, indicating that sufficiently large solitons have very small velocities, while their amplitudes are strongly correlated between different realizations. The right inset in panel (a) demonstrates the ensemble-averaged PDF of soliton amplitudes $\mathcal{P}(\chi)$, which looks rough since different realizations have very close sets of soliton amplitudes.

Figure (a) effectively shows that for universal adiabatic regime we every time grow the same soliton gas irrespective of the Fourier phases of the initial noise.

Hypothesis: for adiabatic regime, phases of different solitons within the same wavefield are uncorrelated.

4. Results – IST spectra, non-adiabatic and non-universal regimes.

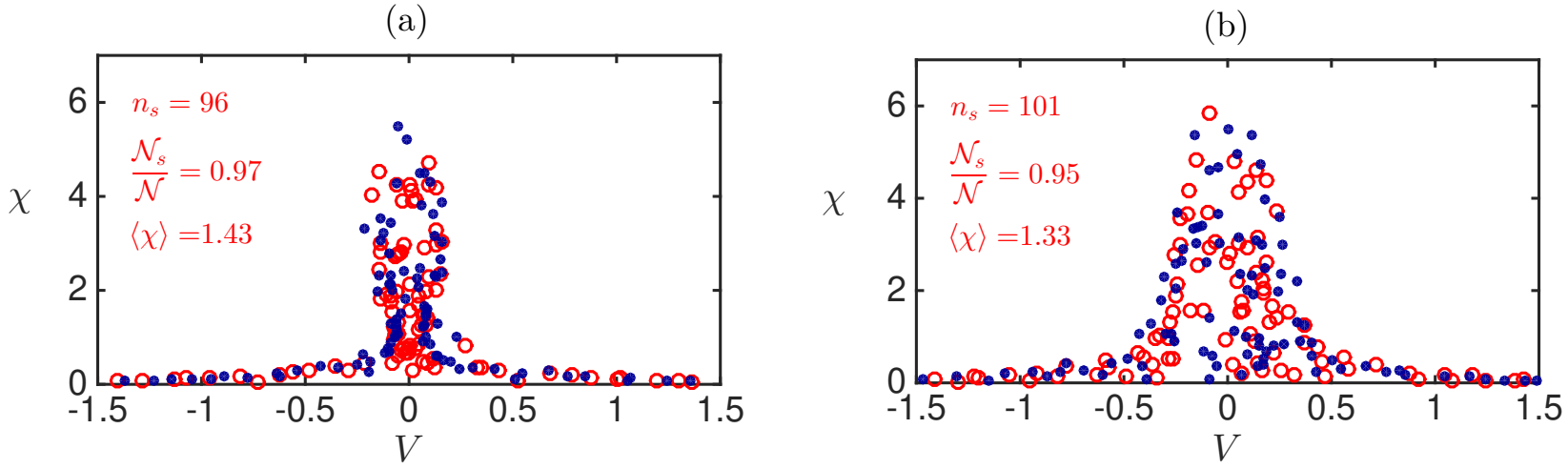

Figure 12: Amplitude-velocity diagrams of solitons at the end of the growth stage for the experiments with (a) non-universal adiabatic regime with $A_0 = 6 \times 10^{-2}$ and (b) non-adiabatic regime with $p_0 = 32 \times 10^{-5}$.

Main distinctions from the universal adiabatic regime:

1) Distribution of soliton amplitudes is significantly wider with $\max \chi \simeq 6$ (non-universal adiabatic regime – presence of solitons in the initial noise and different action of the pumping on the solitonic and non-solitonic contents? non-adiabatic regime – self-organization?).

2) Even at the end of the growth stage $A_f = 1$ large solitons still have noticeable velocities; i.e., the solitonic states are still relatively far from being bound.

3) For both experiments, different realizations of the grown-up wavefield exhibit rather different amplitude-velocity diagrams of their solitonic content.

5. Conclusions.

1. We have studied numerically the integrable turbulence in the framework of the 1D-NLSE model using a new approach called "growing of turbulence". In this approach, a small linear pumping term is added to the equation and the evolution is started from statistically homogeneous Gaussian noise of small amplitude. After reaching a certain level of average intensity, the pumping is switched off and the resulting integrable turbulence is examined.

2. For sufficiently small initial noise and pumping coefficient, and also for not very wide simulation box (basin length), we have found that the turbulence grows in a universal adiabatic (quasi-stationary) regime, with the growth trajectory not depending on the amplitude of the initial noise, pumping coefficient or basin length. There are also non-universal adiabatic regime, with its trajectory depending on amplitude of the initial noise, and non-adiabatic regime which goes through non-stationary statistical states.

3. We have focused on the universal adiabatic regime and studied its growth trajectory from weak nonlinearity through the states of intermediate nonlinearity to strongly nonlinear states. We have observed how wave statistics in these states changes from Gaussian to strongly non-Gaussian with a strong presence of rogue waves. Using the IST method to monitor this evolution, we have found that the solitonic part of the wavefield becomes dominant even when the (linear) dispersion effects are still leading in the dynamics and with increasing average intensity the wavefield approaches a dense bound-state soliton gas, whose properties are defined by the Fourier spectrum of the initial noise.

4. Regimes deviating from the universal adiabatic growth also lead to solitonic states, but solitons in these states have noticeably different velocities and a significantly wider distribution by amplitude, while the appearance of rogue waves is much more frequent.

5. Conclusions – unexpected results.

1. Conditions for adiabatic growth contain relation between the pumping coefficient and basing length. Significance: it is very difficult to create adiabatic regime for large basins.

2. Existence of a non-universal adiabatic regime when (i) the initial noise is sufficiently small, so that the initial state is close to stationary and the adiabatic growth from this state is realized, but (ii) the growth trajectory still depends on noise amplitude. We think that this is happening due to the presence of solitons in the initial noise and the different effect of pumping on the solitonic and non-solitonic contents of the wavefield.

3. For the universal adiabatic regime: no enhanced rogue wave generation until $A_f > 0.5$ and potential-to-kinetic energy ratio $\alpha > 1$.

4. Solitons start to dominate early: already for $A_f = 0.125$ ($\alpha = 0.0625$) we have 60% of all wave action sitting in solitons, and for $A_f = 0.25$ ($\alpha = 0.25$) we have 90% of all wave action stored in the solitonic content. Regimes deviating from the universal adiabatic regime lead to the same number and fraction of solitons in the total wave action. Significance: soliton gas may be much more common in nature than we used to think.

5. As the pumping continues, we observe that solitons increase in number and amplitude and form a bound state soliton gas. Moreover, for the universal adiabatic regime, we always grow the same soliton gas (with the same soliton amplitudes and velocities), which depends only on the Fourier amplitudes of the initial noise but does not depend on specific set of random Fourier phases.

6. References.

1) D.S. Agafontsev, V.E. Zakharov, *Growing of integrable turbulence*, Fiz. Nizk. Temp. **46**, 934–939 (2020).

2) D.S. Agafontsev, A.A. Gelash, R.I. Mullyadzhanov and V.E. Zakharov, *Bound-state soliton gas as a limit of adiabatically growing integrable turbulence*, Chaos Solitons Fractals **166**, 112951 (2023).

Thank you for your attention!